Bidirectional Alterations in Cerebellar Synaptic Transmission of *tottering* and *rolling* Ca^{2+} Channel Mutant Mice

Kaori Matsushita,[1,4] Minoru Wakamori,[1,5] Im Joo Rhyu,[6] Tatsuo Arii,[2,4] Sen-ichi Oda,[7] Yasuo Mori,[3,4] and Keiji Imoto[1,4]

[1]Department of Information Physiology and [2]Center for Brain Experiment, National Institute for Physiological Sciences, [3]Center for Integrative Bioscience, Okazaki National Research Institutes, and [4]School of Life Science, the Graduate University for Advanced Studies, Okazaki 444-8585, Japan, [5]Department of Physiology, Kagoshima University Faculty of Medicine, Kagoshima 890-8520, Japan, [6]Department of Anatomy, Korea University College of Medicine, Seoul 136-705, Korea, and [7]Laboratory of Animal Management, School of Agricultural Sciences, Nagoya University, Nagoya, Aichi 464-8601, Japan

Hereditary ataxic mice, *tottering* (*tg*) and *rolling* Nagoya (*tg^{rol}*), carry mutations in the P/Q-type Ca^{2+} channel α_{1A} subunit gene. The positions of the mutations and the neurological phenotypes are known, but the mechanisms of how the mutations cause the symptoms and how the different mutations lead to various onset and severity have remained unsolved. Here we compared fundamental properties of excitatory synaptic transmission in the cerebellum and roles of Ca^{2+} channel subtypes therein among wild-type control, *tg*, and *tg^{rol}* mice. The amplitude of EPSC of the parallel fiber–Purkinje cell (PF-PC) synapses was considerably reduced in ataxic *tg^{rol}*. Although the amplitude of the parallel fiber-mediated EPSC was only mildly decreased in young non-ataxic *tg* mice, it was drastically diminished in adult ataxic *tg* mice of postnatal day 28–35, showing a good correlation between the impairment of the PF-PC synaptic transmission and manifestation of ataxia. In contrast, the EPSC amplitude of the climbing fiber–Purkinje cell (CF-PC) synapses was preserved in *tg*, and it was even increased in *tg^{rol}*, which was associated with altered properties of the postsynaptic glutamate receptors. The climbing fiber-mediated EPSC was more dependent on other Ca^{2+} channel subtypes in mutant mice, suggesting that such compensatory mechanisms contribute to maintaining the CF-PC synaptic transmission virtually intact. The results indicate that different mutations of the P/Q-type Ca^{2+} channel not only cause the primary effect of different severity but also lead to diverse additional secondary effects, resulting in disruption of well balanced neural networks.

Key words: calcium channel; synaptic transmission; mutant mice; tottering *mice;* rolling *Nagoya mice; cerebellar ataxia; glutamate receptor*

Ca^{2+} controls diverse cellular processes, which include neurotransmitter release, gene expression, and cell proliferation (Tsien and Tsien, 1990; Ghosh and Greenberg, 1995). To evoke these responses, multiple voltage-gated Ca^{2+} channel types, including five high-threshold types (L, N, P, Q, and R) and the low-threshold T-type, form major Ca^{2+} entry pathways (Catterall, 2000). Several of these are colocalized in a single neuron and are assumed to contribute to fine tuning of activity. Although the critical role of Ca^{2+} channels, particularly the P/Q- and N-types, for neurotransmitter release is established (Hirning et al., 1988; Turner et al., 1992; Takahashi and Momiyama, 1993; Artalejo et al., 1994; Regehr and Mintz, 1994), their role in signal integration or synaptic plasticity is poorly understood.

Voltage-gated Ca^{2+} channels are composed of the main pore-forming α_1 subunit, encoded by a family of genes, and the accessory α_2/δ, β, and γ subunits (Catterall, 2000). The α_{1A} subunit was originally characterized as a high-voltage-activated Ca^{2+} channel insensitive to the N-type-selective inhibitor ω-conotoxin GVIA (ω-CgTx) and the L-type inhibitor dihydropyridine (Mori et al., 1991). It is now accepted that the P- and Q-types, which differ in ω-agatoxin-IVA (ω-Aga-IVA) sensitivity and inactivation kinetics (Llinás et al., 1989; Regan et al., 1991; Mintz et al., 1992; Zhang et al., 1993), are produced from the single α_{1A} gene by alternative splicing (Mori et al., 1991; Sather et al., 1993; Bourinet et al., 1999) and/or through association with different isoforms of accessory subunits (Stea et al., 1994).

Recent studies have determined that mutations of the Ca^{2+} channel α_{1A} subunit gene are associated with cerebellar ataxia and other neurological disorders in mice (Fletcher et al., 1996) and human (Ophoff et al., 1996). The *tottering* (*tg*) mice (Green and Sidman, 1962) have a mutation in the extracellular region of the second repeat (Fletcher et al., 1996). The *rolling* Nagoya (*tg^{rol}*) mice (Oda, 1973) have a mutation in the voltage-sensing S4 segment of the third repeat (Mori et al., 2000). The *leaner* (*tg^{la}*) mice (Sidman et al., 1965) have a mutation in a splice donor consensus sequence, resulting in altered C-terminal sequences (Fletcher et al., 1996). Although ataxia is the common symptom among the mutant mice, its severity differs significantly; *tg* mice show the mildest ataxia, whereas it is most severe in *tg^{la}* mice (Herrup and Wilczynski, 1982).

Neuronal circuits of the cerebellar cortex have been well characterized (Llinás and Walton, 1998). The cerebellar cortex receives inputs from two main sources, mossy fibers and climbing

Received Feb. 13, 2002; accepted March 18, 2002.

This work was supported by research grants from the Ministry of Education, Culture, Sports, Science and Technology of Japan and the Japan Society for the Promotion of Science. We thank Drs. Masanobu Kano, Toshihiko Momiyama, and Akiko Momiyama for helpful suggestions and Naomi Sekiguchi for excellent technical support.

Correspondence should be addressed to Keiji Imoto, Department of Information Physiology, National Institute for Physiological Sciences, Okazaki 444-8585, Japan. E-mail keiji@nips.ac.jp.

Copyright © 2002 Society for Neuroscience 0270-6474/02/224388-11$15.00/0

fibers. The mossy fiber system originates from various sources and provides, through granule cells, numerous parallel-fiber inputs on the terminal regions of Purkinje cell dendrites. In contrast, one climbing fiber originating in the inferior olive innervates the apical dendrite of a single Purkinje cell. Ca^{2+} channel dysfunction, therefore, may affect the cerebellar excitatory synaptic inputs, which consequently may cause dysfunction of cerebellar circuits. In this study, we studied the basic properties of excitatory synaptic transmission in the parallel fiber–Purkinje cell (PF-PC) and climbing fiber–Purkinje cell (CF-PC) synapses of wild-type control (wt), *tg*, and *tg^{rol}*.

MATERIALS AND METHODS

Animals. The C57BL/6J-*tg* strain of *tg* mice was introduced from the Jackson Laboratory (Bar Harbor, ME). The *tg* and *tg^{rol}* mice were provided with a commercial diet (CE-2, Nihon Clea, Tokyo, Japan) and water *ad libitum* under conventional conditions with controlled temperature, humidity, and lighting (22 ± 2°C, 55 ± 5%, and 12 hr light/dark cycle with lights on at 7 A.M.). These strains were maintained and propagated by mating between heterozygous mice in the Center for Experimental Animal, Okazaki National Research Institutes.

PCR-restriction fragment length polymorphism genotyping. Genotyping of *tg* mice was performed using PCR-restriction fragment length polymorphism (PCR-RFLP). A PCR fragment was obtained using a pair of primers, 5′-GGAAACCAGAAGCTGAACCA-3′ (sense) and 5′-GAAATGGAGGAATTCAGGG-3′ (antisense) and genomic DNA as a template. Digestion of the fragment with *Aci*I yielded the following fragments: 295 bp in *tg*/*tg*, 127 and 168 bp in +/+, and 127, 168, and 295 bp in *tg*/+ (Wakamori et al., 1998). Because *tg^{rol}*/*tg^{rol}* mice exhibit overt ataxia at 2 weeks of age, it was not necessary to conduct genotyping using the molecular biological methods.

Slice preparation. Mice were killed by decapitation under halothane general anesthesia, in accordance with the institutional guideline for animal experiments. Brains were removed from wt, *tg*, and *tg^{rol}* mice at postnatal days (P) 14–20 and from wt and *tg* mice at P28–35 and cooled in ice-cold saline (described below). Parasagittal 250-μm-thick slices were cut from the cerebellar vermis with a Vibratome (DTK-1000; Dosaka, Kyoto, Japan). Slices were kept at room temperature for 1 hr after slicing in artificial CSF (ACSF) containing (in mM): 125 NaCl, 25 $NaHCO_3$, 25 glucose, 2.5 KCl, 1.25 NaH_2PO_4, 2 $CaCl_2$, and 1 $MgCl_2$, bubbled with carbogene (95% O_2 and 5% CO_2).

Electrophysiology of slice preparations. After 1 hr incubation at room temperature, slices were transferred to a recording chamber and perfused with ACSF. Bicuculline (10 μM) was always present in the saline to block spontaneous IPSCs. A whole-cell voltage-clamp recording was made from Purkinje cells, which were visually identified using an upright microscope (Axioskop FS, Carl Zeiss, Jena, Germany) equipped with a 60× water immersion objective (Olympus Optical, Tokyo, Japan) and an infrared differential interference contrast video system (C2400–07, Hamamatsu Photonics, Hamamatsu, Japan) (Edwards et al., 1989; Llano et al., 1991). Patch pipettes were made from borosilicate capillaries (2.0 mm outer diameter and 1.0 mm inner diameter; Hilgenberg, Malsfeld, Germany). The resistance of patch pipettes was 3–5 MΩ when filled with an intracellular solution that contained (in mM): 100 Cs-gluconate, 34.5 CsCl, 4 NaCl, 10 HEPES, 4 Mg-ATP, 0.3 Na-GTP, 10 EGTA (adjusted to pH 7.3 with CsOH). QX-314 (final 5 mM) was added to prevent Na^+ spike generation. EPSCs were recorded with an EPC7 patch-clamp amplifier (List-Medical-Electronics, Darmstadt, Germany). Stimulation and data acquisition were performed using the PULSE program (version 7.5, HEKA Elektronik, Lambrecht, Germany). The signals were filtered at 3 kHz and digitized at 20 kHz. The experiments were performed at a bath temperature of 32°C.

Somatic whole-cell voltage recording in the current-clamp mode was made with 4–8 MΩ patch pipettes using the EPC-7 amplifier. The patch pipettes were filled with the following internal solution containing (in mM): 135 K-gluconate, 20 KCl, 2 $MgCl_2$, 2 Na_2ATP, 0.3 NaGTP, 0.2–0.5 EGTA, and 10 HEPES (pH was adjusted to 7.3 with KOH). Patch pipette resistance was 5–10 MΩ. After the whole-cell configuration was established, the membrane potential was maintained at −70 mV by injecting a constant current ranging between 50 and 250 pA. During the experiments, input resistance was periodically monitored by measuring the steady-state current evoked by 10 mV pulses in a Purkinje cell voltage clamped at −70 mV. Cells were rejected if input resistance decreased below 80 MΩ. The signals were filtered at 3 kHz and digitized at 50 kHz. The experiments were performed at a bath temperature of 32°C.

Parallel fiber response. Parallel fiber-mediated EPSCs (PF-EPSCs) were evoked by electrical stimulation, using a bipolar electrode with a tip diameter of 13 μm made from a theta-shaped glass capillary (TGC200, Clark Electromedical Instruments, Reading, England) and filled with 1 M NaCl (DC resistance ~3 MΩ). Square pulses of 100 μsec duration and amplitude ranging from 1.5 to 12 V were applied at 0.2 Hz, unless specified otherwise, while the stimulation glass pipette was moved within the visual field until the synaptic current was evoked with minimum stimulus intensity. The stimulation pipette was usually placed at ~100 μm from the pial surface. The holding potential was adjusted in every experimental condition to make the driving force constant (70 mV) for inward currents. Evoked EPSC amplitude was compared among wt, *tg*, and *tg^{rol}* at P14–20 or P28–35.

Climbing fiber response. Climbing fiber-mediated EPSCs (CF-EPSCs) were evoked by electrical stimulation, using a bipolar theta-shaped capillary electrode (with a tip diameter of 10–13 μm) filled with 1 M NaCl. The pipette was placed in the granule cell layer at 50–100 μm from the soma of a Purkinje cell where EPSCs were measured. Square pulses (duration 100 μsec, amplitude 1–10 V) were applied at 0.1 Hz, unless specified otherwise. The holding potential was set in every experimental condition to make the driving force constant (20 mV) for inward currents. The evoked EPSC amplitudes were compared among wt, *tg*, and *tg^{rol}* at P14–20 or P28–35.

Because the large size of CF-EPSCs and the extensive dendritic arbor of Purkinje cells make voltage clamp of these currents technically difficult, we adopted several strategies to optimize the quality of voltage clamp and to minimize the errors involved. First, P14–20 mice (mainly P17) were used, because at this age the Purkinje cell dendritic arbor is less extensive than in the adult, and CF innervation is located on the soma and proximal dendrites (Altman and Bayer, 1997). Second, the electrode resistance was minimized by using large electrodes (3–4 MΩ) combined with series resistance compensation (50–70%). Series resistance was monitored by measuring the transient current evoked by 10 mV pulses in a Purkinje cell held at −70 mV. Cells were rejected if it increased above 20 MΩ. Third, recordings were made at depolarized voltages so that the amplitudes of synaptic currents were reduced and voltage-gated channels were inactivated. We measured the current reversal potential before and after the measurements and discarded the measurements if the reversal potential shifted by >5 mV.

Changes in glutamate concentration in the synaptic cleft were assessed by measuring the suppressing effect on the CF-EPSC amplitude of various concentrations of a partial AMPA receptor antagonist, γ-D-glutamylglycine (γ-DGG).

We observed innervation of multiple climbing fibers in only a few wt and *tg* Purkinje cells, but we observed multiple innervation more frequently in *tg^{rol}* Purkinje cells. In this study, we excluded Purkinje cells with multiple innervation from the analyses.

Miniature CF-EPSCs. For recording miniature CF-EPSCs, we used mouse brains from P14–20 and P28–35 wt, ataxic *tg^{rol}*, and *tg.* After establishing a stable condition for CF-EPSC measurements, we changed external solutions from ACSF to a Sr^{2+}-containing solution that was composed of (in mM): 125 NaCl, 25 $NaHCO_3$, 25 glucose, 2.5 KCl, 1.25 NaH_2PO_4, 5 $SrCl_2$, and 5 $MgCl_2$ (Silver et al., 1998). The holding potential was −70 mV. Climbing fibers were stimulated at 0.2 Hz. Series resistance and reversal potential were measured periodically. We analyzed synaptic events >40 pA in peak amplitude in a 100 msec time window starting 200 msec after stimulation. The decay phase of synaptic events was fitted with a single exponential.

Preparation of dissociated Purkinje cells. Purkinje cells were freshly dissociated from *tg*, *tg^{rol}*, and wt at P20–32. The procedure for obtaining dissociated cells from mice was similar to that described previously (Wakamori et al., 1993). Coronal slices (400 μm thick) of the cerebellum were prepared using the vibratome. After preincubation in Krebs' solution for 40 min at 31°C, the slices were digested, first in Krebs' solution containing 0.01% pronase (Calbiochem-Novabiochem, La Jolla, CA) for 25 min at 31°C and then in solution containing 0.01% thermolysin (protease, type X; Sigma, St. Louis, MO) for 25 min at 31°C. The Krebs' solution used for preincubation and digestion contained the following (in mM): 124 NaCl, 5 KCl, 1.2 KH_2PO_4, 2.4 $CaCl_2$, 1.3 $MgSO_4$, 26 $NaHCO_3$, and 10 glucose. The solution was oxygenated continuously with 95% O_2 and 5% CO_2. Then the Purkinje cell layer of the brain slices was punched out and dissociated mechanically by the use of fine glass pipettes having a tip diameter of 100–200 μm. Dissociated cells settled on tissue culture

dishes (Primaria 3801, Nippon Becton Dickinson, Tokyo, Japan) within 30 min. Purkinje cells were identified by their large diameter and characteristic pear shape because of the stump of the apical dendrite. To make a sufficient space-clamp of the Purkinje cell body, Purkinje cells lacking most of dendrites were used throughout the present experiments.

Whole-cell recordings of dissociated Purkinje cells. Electrophysiological measurements were performed on acutely dissociated Purkinje cells. Currents were recorded at room temperature (22–25°C) using whole-cell mode of the patch-clamp technique with an Axopatch 200B patch-clamp amplifier (Axon Instruments, Foster City, CA). Patch pipettes were made from borosilicate glass capillaries (1.5 mm outer diameter and 0.87 mm inner diameter; Hilgenberg). The patch electrodes were fire polished. Pipette resistance ranged from 1 to 2 MΩ when filled with the pipette solutions described below. The series resistance was electronically compensated to >70%. Currents were sampled at 5 kHz after low-pass filtering at 1 kHz (−3 dB). Data were collected and analyzed using the pClamp 6.02 software (Axon Instruments). The external solution contained (in mM): 140 NaCl, 5 KCl, 2 $CaCl_2$, 10 glucose, 10 HEPES (adjusted to pH 7.4 with Tris). The pipette solution contained (in mM): 140 CsCl, 10 EGTA; pH was adjusted to 7.2 with CsOH. Rapid application of drugs was made by a modified "Y-tube" method (Wakamori et al., 1998). The external solution surrounding a recorded cell was completely exchanged within 200 msec.

Estimation of fractional contribution of Ca^{2+} channel subtypes. The nonlinear relationship between the presynaptic Ca^{2+} concentration and the postsynaptic current amplitude has been described at various synapses (Dodge and Rahamimoff, 1967). A small decrease in presynaptic Ca^{2+} entry can cause a large reduction in the synaptic responses. The relative contributions of Ca^{2+} channel subtypes to EPSCs were estimated using a power relation: $I = (a + b + c)^m$, where I is the normalized EPSC amplitude, and a, b, and c represent the fractions of presynaptic Ca^{2+} channel subtypes sensitive to ω-Aga-IVA and ω-CgTx and the fraction insensitive to both toxins, respectively. The value m is the power coefficient and is assumed to be 3. The relative amplitude of postsynaptic currents remaining after application of ω-Aga-IVA (A), ω-CgTx (B), and both toxins (C) can be described as $A = (1 - a)^m$, $B = (1 - b)^m$, and $C = c^m$, respectively, using $a + b + c = 1$.

In addition, the Hill's equation, $I = A\ (a + b + c)^m/\{(a + b + c)^m + d^m\}$, is used for CF-EPSC (Momiyama and Koga, 2001) to take the saturation effect of Ca^{2+} binding sites into consideration, where A is a scaling factor, and d indicates a Ca^{2+} influx/concentration relative to $a + b + c$, at which CF-EPSC amplitude is half-maximal. Because I is a normalized amplitude, A can be described by the equation $A = 1 + d^m$. The power factor of $m = 4$ and the value of the relative half-saturation concentration of $d = 0.6$ were used to fulfill the condition $a + b + c = 1$.

To validate the estimates of contributions of Ca^{2+} channel subtypes, we examined the effect on PF-EPSC and CF-EPSC amplitudes of lowering the extracellular Ca^{2+} concentration from 2.0 mM (control) to 0.5 mM. The concentration of divalent cations was kept constant by the increasing Mg^{2+} concentration. The PF-EPSC and CF-EPSC amplitudes were normalized to the values with 2.0 mM Ca^{2+}, plotted against the extracellular Ca^{2+} concentration, and fit by the power relation or the Hill's equation.

Data analysis and statistics. All values are given as means ± SE. Statistical comparison between normal and mutant mice or mutant channels was performed by t test ($^*p < 0.05$, $^{**}p < 0.01$). Data analysis and fitting procedures were performed using the IgorPro program (Wavemetrics, Lake Oswego, OR). To obtain mean values, the values of EPSC peak amplitude, rise-time, and decay time constant were obtained from each of 5–10 consecutive traces and were averaged. The decaying phase of EPSCs was fit with a single exponential.

Chemicals. Bicuculline, 6-cyano-7-nitroquinoxialine-2,3-dione (CNQX), (±)-2-amino-5-phosphonopentanoic acid (APV), and γ-DGG were obtained from Sigma (St. Louis, MO). Peptide toxins ω-Aga-IVA and ω-CgTx were obtained from Peptide Institute (Osaka, Japan). Nifedipine was obtained from Alomone Labs (Jerusalem, Israel). All other chemicals were from Nacalai Tesque (Kyoto, Japan) or Wako Pure Chemical Industries (Osaka, Japan), unless specified otherwise. Stock solutions were made in distilled water or dimethylsulfoxide (for nifedipine, the concentration of dimethylsulfoxide in the final solution was 0.1%). ω-CgTx and ω-Aga-IVA were coapplied with 1 mg/ml cytochrome c from horse heart (Nacalai Tesque) to prevent unspecific binding of the peptide toxins. Nifedipine was protected from light.

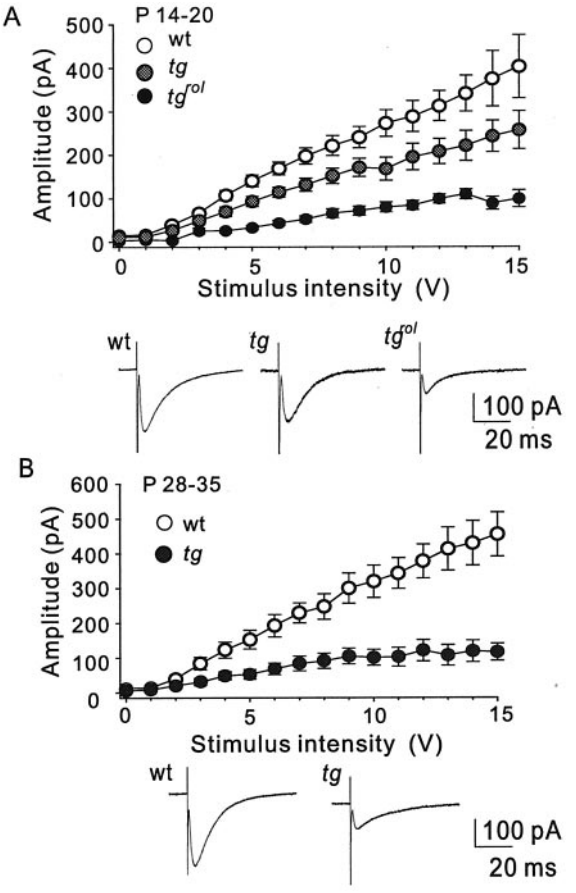

Figure 1. PF-PC synaptic transmission in mutant mice. *A*, PF-EPSC peak amplitudes were plotted against the intensity of stimulation for wt and mutant mice at P14–20. Mean peak amplitudes ± SEM from 10 wt, 7 *tg*, and 7 tg^{rol} Purkinje cells are shown. *Insets* show traces of PF-EPSCs from wt (*left*), *tg* (*middle*), and tg^{rol} (*right*) Purkinje cells. Each trace is an average of 10 current recordings. *B*, The PF-EPSC peak amplitude–stimulus intensity relationship, as in *A*, from 8 wt and 10 *tg* Purkinje cells (*P28–35*). *Insets* show traces of PF-EPSC from wt (*left*) and *tg* (*right*) Purkinje cells evoked by 10 V stimulation. Each trace is an average of 10 current recordings.

RESULTS

EPSCs at parallel fiber–Purkinje cell synapses in mutant mice

Homozygous tg^{rol} mice start showing ataxic behaviors around P10, whereas homozygous *tg* mice do not show ataxic symptoms until 3~4 weeks of age. We recorded PF-EPSCs in the whole-cell configuration from Purkinje cells in parasagittal cerebellar slices and compared them among wt, *tg*, and tg^{rol} at P14–20 or P28–35. A Purkinje cell receives inputs from a large number of parallel fibers, but focal stimulation in the molecular layer activates only a very limited number of parallel fibers. This fact made it difficult to compare PF-EPSC amplitudes in different slice preparations. To circumvent this problem, we stimulated parallel fibers at geometrically determined locations and changed intensity of stimulation to obtain the current amplitude–stimulation intensity relationship.

PF stimulation evoked EPSCs, of which amplitudes increased almost linearly with increments of stimulation intensity in wt and mutant mice (Fig. 1*A*). However, PF stimulation was consistently less effective in eliciting PF-EPSCs in Purkinje cells of *tg* and

Table 1. Basic properties of PF-EPSCs in mutant mice

	Amplitude (pA)	Decay time constant (msec)	10–90% Rise time (msec)	Paired-pulse ratio (%)
Mice (P14–20)				
wt	272.6 ± 30.4 (14)	12.1 ± 1.3 (14)	1.82 ± 0.16 (10)	165.3 ± 7.9 (11)
tg	168.3 ± 26.4* (14)	12.0 ± 0.8 (14)	2.26 ± 0.21 (10)	181.9 ± 6.0 (10)
tg^{rol}	79.6 ± 11.7* (10)	12.9 ± 1.6 (10)	2.44 ± 0.34 (10)	212.8 ± 18.7* (10)
Mice (P28–32)				
wt	319.4 ± 21.3 (10)	12.4 ± 1.4 (10)	2.08 ± 0.29 (10)	158.9 ± 4.5 (10)
tg	88.76 ± 46.3 (10)	13.0 ± 2.3 (10)	2.22 ± 0.52 (10)	159.6 ± 9.7 (10)

PF-EPSCs were evoked by 10 V stimulation. All data are expressed as mean ± SEM. Numbers of recorded Purkinje cells are shown in the parentheses. The decay time constant was obtained by fitting the EPSC decay with a single exponential. Paired-pulse ratio is second EPSC/first EPSC. Interpulse interval is 50 msec. *$p < 0.05$.

ataxic tg^{rol} than in wt Purkinje cells ($p < 0.05$) in the stimulation intensity range from 3 to 15 V. Moreover, although PF-EPSCs of P14–20 *tg* mice, which do not have obvious ataxia, showed ~30% reduction in amplitude, PF-EPSC amplitude exhibited a more dramatic reduction (~70%) in clearly ataxic *tg* mice at P28–35 (Fig. 1*B*). The current–voltage (*I–V*) relationship for PF-EPSCs was linear in the three groups of mice (data not shown). These results demonstrate that PF-PC synaptic transmission is unambiguously impaired in *tg* and tg^{rol} mice and that the degree of the amplitude reduction correlates with the severity of the ataxic symptom.

Properties of PF-EPSCs

We measured the 10–90% rise time and the decay time constant of PF-EPSCs, obtained at the stimulus intensity of 10 V (Table 1). The decay phase was fitted with a single exponential function. Both parameters were not significantly different among wt, *tg*, and tg^{rol} mice, indicating that the mutations of the P/Q-type Ca^{2+} channel gene do not influence the kinetics of PF-EPSCs. PF-EPSCs could be blocked by CNQX (10 μM) but were insensitive to an NMDA receptor antagonist, APV (100 μM) (data not shown), demonstrating that PF-EPSCs in Purkinje cells are mediated exclusively by non-NMDA receptors even in mutant mice, as reported previously in rat (Konnerth et al., 1990) and mouse (Aiba et al., 1994; Kano et al., 1995).

PF-EPSCs are known to exhibit a prominent paired-pulse facilitation (PPF). The PPF magnitudes in the tg^{rol} were significantly greater than wt or *tg* at 50 msec interpulse intervals (Fig. 2*A*,*B*). Because PPF is considered to reflect the amount of residual Ca^{2+} in presynaptic terminals (Zucker, 1989), this finding suggests that the amount of Ca^{2+} influx into the tg^{rol} nerve terminal evoked by a single activation is too small for reliable synaptic transmission, but the PPF magnitudes in the ataxic *tg* at P28–35 were no larger than that of wt, suggesting that the change in PPF itself is not directly related to the ataxic symptom (Fig. 2*A*,*C*).

Ca^{2+} channel subtypes in PF-PC synapses

Previous studies of synaptic transmission at the rat cerebellar PF-PC synapse indicate that both N- and P/Q-type channels are involved in the release of neurotransmitter (Mintz et al., 1995). Because the *tg* and tg^{rol} mutations decrease the P/Q-type Ca^{2+} channel currents at presynaptic terminals, less reliance of neurotransmitter release on the P/Q-type channel and more reliance on the N-type channel would be expected. Application of 0.2 μM ω-Aga-IVA to the wt slices almost abolished the synaptic currents in Purkinje neurons; on average, the PF-EPSCs were reduced by ~90% (Fig. 3*A*,*C*; Table 2). On the other hand, application of 3 μM ω-CgTx to the wt slices only partially blocked PF-EPSCs, reducing them by ~20% (Fig. 3*B*,*D*; Table 2). The remaining component after application of both toxins was ~10%. Because the remaining component was not affected by nifedipine (10 μM), an L-type Ca^{2+} channel blocker, it likely corresponds to the R-type Ca^{2+} channel. Therefore, the wt PF terminals contain the

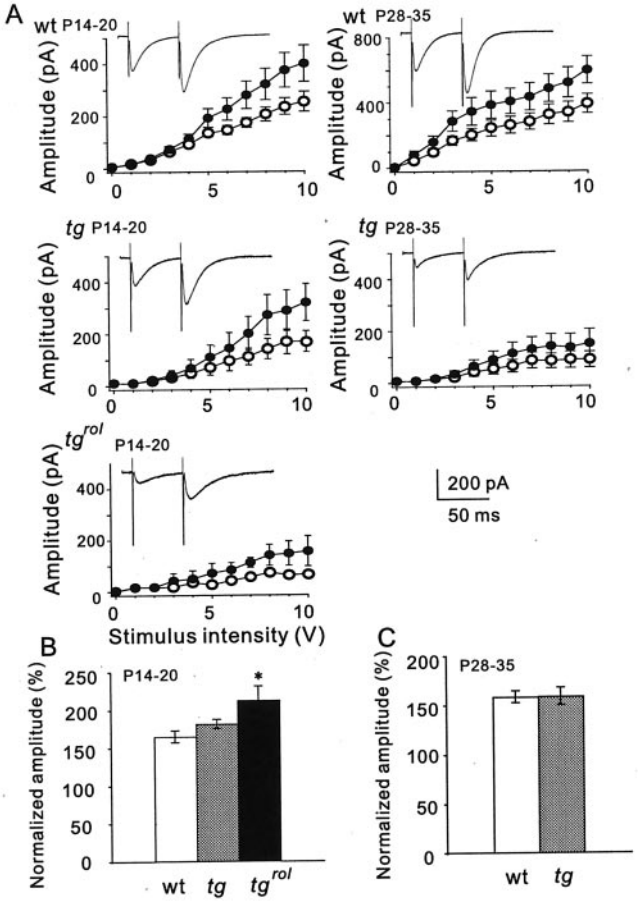

Figure 2. Paired-pulse facilitation in PF-EPSC. *A*, The PF-EPSC peak amplitude–stimulus intensity relations for paired-pulse stimulation (interval 50 msec) of wt and mutants. Mean peak amplitudes evoked by the first stimulation (○) and the second stimulation (●) were obtained from 10 measurements. Calibration is common for all traces. *Insets* show typical current traces evoked by 10 V stimulation (average of 10 recordings). *B*, Mean paired-pulse ratio (second EPSC/first EPSC) from wt, *tg*, and tg^{rol} at P14–20 (10 Purkinje cells each). *C*, Mean paired-pulse ratio from wt and *tg* at P28–35 (10 Purkinje cells each). Error bars represent SEM in *A–C*.

Table 2. PF-EPSC synaptic current fractions after application of Ca^{2+} channel-blocking toxins

Toxins applied	ω-Aga-IVA (*a*)	ω-CgTx (*b*)	ω-Aga-IVA + ω-CgTx (*c*)	(*a* + *b* + *c*)
wt	0.09 ± 0.01 (0.55)	0.76 ± 0.04 (0.09)	0.08 ± 0.01 (0.43)	(1.07)
tg	0.17 ± 0.02 (0.45)	0.43 ± 0.04 (0.24)	0.19 ± 0.05 (0.56)	(1.25)
tg^{rol}	0.17 ± 0.02 (0.44)	0.61 ± 0.05 (0.15)	0.23 ± 0.03 (0.61)	(1.20)

Each value represents mean ± SEM of three or four measurements. Numbers in parentheses (*a–c*) are the estimated fractions of the Ca^{2+} channel subtypes mediating synaptic transmission, assuming a third power relation between presynaptic Ca^{2+} concentration and postsynaptic response amplitude.

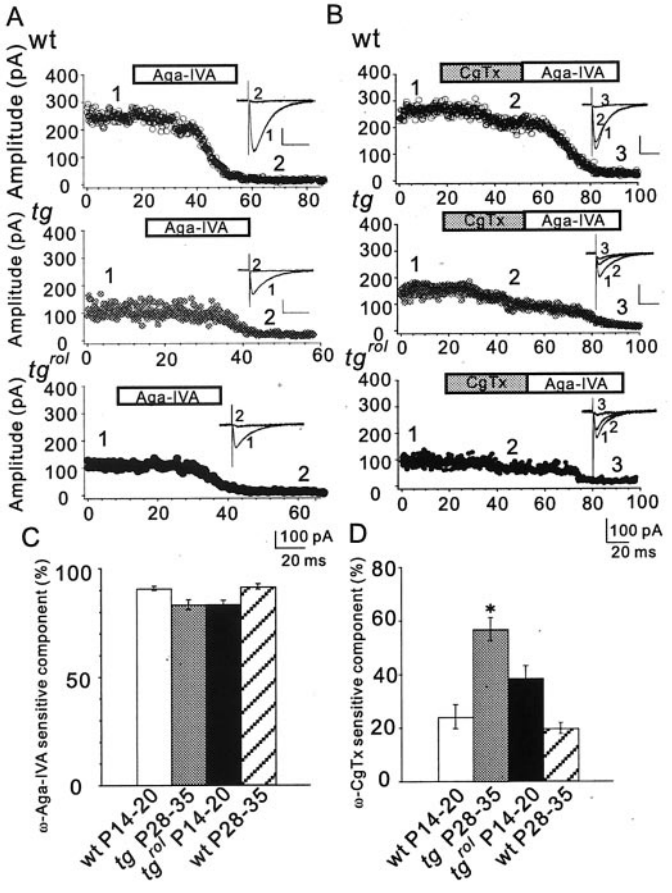

Figure 3. Toxin sensitivity of PF-EPSC. *A*, *B*, Time courses of the peak PF-EPSC amplitude in response to application of 0.2 μM ω-Aga-IVA (*A*) and 3 μM ω-CgTx and subsequent 0.2 μM ω-Aga-IVA (*B*). *Insets* show current traces at the time indicated by the *numbers*. Each trace is an average of 10 recordings. *C*, *D*, The ω-Aga-IVA-sensitive (*C*) and the ω-CgTx-sensitive (*D*) components (mean ± SEM) of PF-EPSC of wt, *tg*, and tg^{rol} from three to six measurements.

P/Q-, N-, and presumed R-type Ca^{2+} channels, but the P/Q-type plays the predominant role.

When the same set of experiments was performed on *tg* and tg^{rol} mice (Fig. 3; Table 2), application of ω-Aga-IVA caused a large decrease in PF-EPSC amplitude similarly in *tg* and tg^{rol} mice, but the reduction was smaller than in wt mice. In contrast to the small reduction by ω-CgTx in wt, there was a large decrease of ~60% in PF-EPSC amplitude in *tg*. A large reduction in PF-EPSCs, although to a lesser extent, was also observed in tg^{rol}. The remaining component after application of both toxins was larger in *tg* and tg^{rol} than that of wt.

The sum of the ω-Aga-IVA- and ω-CgTx-sensitive EPSC fractions and the EPSC fraction insensitive to both is larger than unity, showing an apparent overlap in the effect of ω-Aga-IVA and ω-CgTx on the synaptic currents. This apparent overlap can be explained by a nonlinear relation between the Ca^{2+} influx and EPSCs. In our estimation using a power function from the data of PF-EPSCs, the sum of the estimated Ca^{2+} channel subtype fractions was close to unity (Table 2). The estimated P/Q-type fraction was decreased from 55% in wt to 45% in *tg* and tg^{rol}, whereas the N-type fraction and the assumed R-type fraction increased in the mutants. The increase in the N-type fraction was more prominent in *tg* than in tg^{rol}, which may contribute to the difference in severity of ataxia between *tg* and tg^{rol}.

EPSCs at climbing fiber–Purkinje cell synapses in mutant mice

CF-EPSCs were examined in parasagittal cerebellar slices from wt, *tg*, and tg^{rol} mice at P14–20 and from wt and *tg* at P28–35. Climbing fibers were stimulated locally in the granule cell layer, and CF-EPSCs of Purkinje cells were recorded in the whole-cell configuration. CF-EPSCs could be clearly distinguished from PF-EPSCs by the following two criteria: (1) CF-EPSCs appeared with a discrete step when the stimulus intensity was increased gradually, and (2) CF-EPSCs showed paired-pulse depression (PPD), in contrast to PF-EPSCs that exhibited PPF (Konnerth et al., 1990). In a majority of wt, *tg*, and tg^{rol} Purkinje cells, a large EPSC was elicited in an all-or-none manner without contamination of parallel fiber responses as the stimulus intensity was gradually increased (pulse width 100 μsec, strength 0–100 V). In wt and mutant mice, the *I–V* relationship for the peak current amplitude was linear (data not shown). Although the peak amplitude of CF-EPSCs was unaltered in *tg*, that of tg^{rol} was increased significantly (Fig. 4*A*,*B*). The results of unaltered or enhanced CF-EPSCs were surprising, because we expected reduced CF-EPSCs in ataxic mutant mice, as was the case for PF-EPSCs.

Properties of CF-EPSCs

To examine whether the kinetics of CF-EPSCs were altered in the mutant mice, we measured the 10–90% rise time and the decay time constant of CF-EPSCs in wt and mutant mice (Table 3). Although the 10–90% rise time was not significantly different among wt, *tg*, and tg^{rol} mice, the decay time constant of tg^{rol} was considerably greater than that of wt and *tg*. Thus, the tg^{rol} mutation of the P/Q-type Ca^{2+} channel results in not only an increased CF-EPSC amplitude but also an alteration of CF-EPSC kinetics.

The slower decay time constant in tg^{rol} suggests a possibility that CF-EPSCs may be partly mediated by the NMDA receptor channels, which show slower activation and slower current decay than AMPA receptor channels, but CF-EPSCs were completely insensitive to APV (100 μM) in wt, *tg*, and tg^{rol}, whereas they were blocked by CNQX (10 μM) (data not shown). This result indicates that CF-EPSCs are mediated exclusively by non-NMDA receptors not only in wt and *tg* but also in tg^{rol}, consistent with previous

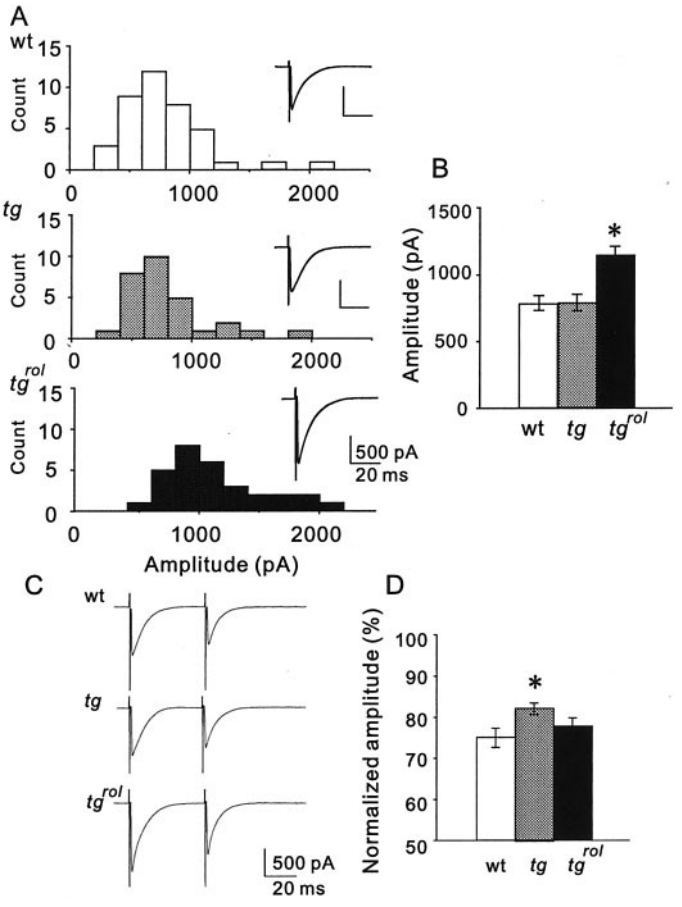

Figure 4. CF-PC synaptic transmission in mutant mice. *A*, The distribution of the CF-EPSC peak amplitude from 40 wt, 30 *tg*, and 31 tg^{rol} Purkinje cells at P14–20. All Purkinje cells were mono-innervated. *Insets* show typical traces of CF-EPSC from wt, *tg*, and tg^{rol} Purkinje cells at P14–20. Three to five traces were averaged. *B*, Mean peak amplitudes of CF-EPSC of wt, *tg*, and tg^{rol} at P14–20. Values are presented as mean ± SEM. $^*p < 0.05$. *C*, CF-EPSCs to pairs of stimuli separated by 50 msec in mono-innervated Purkinje cells of wt, *tg*, and tg^{rol} at P14–20. Three to five traces were averaged. *D*, Paired-pulse ratios (second EPSC/first EPSC; mean ± SEM) from 17 wt, 10 *tg*, and 10 tg^{rol} Purkinje cells. Note that the value of *tg* is larger than wt or tg^{rol} ($^*p < 0.05$).

reports of rat (Konnerth et al., 1990) and mouse (Aiba et al., 1994; Kano et al., 1995).

In contrast to PPF of PF-EPSCs, PPD is a characteristic feature of the CF-PC synapse, which results from decreased transmitter release from presynaptic terminals in response to the second stimulus of a pair (Konnerth et al., 1990). In wt and tg^{rol}, CF-EPSCs exhibited considerable PPD at 50 msec interpulse intervals, but PPD of *tg* CF-EPSCs was significantly smaller than that of the wt or tg^{rol} CF-EPSCs (Fig. 4*C*,*D*; Table 3). Because *tg* mice develop ataxia at ~3 weeks of age, we examined the possible relationship between the reduced PPD and ataxia in ataxic *tg* mice (P28–32). PPD was further reduced in adult ataxic mice compared with non-ataxic young mice, indicating that the reduced PPD itself was not directly related to ataxia. The amplitude, decay time constant, and rise time of ataxic *tg* mice showed no difference (Table 3).

Firing pattern evoked by CF stimulation

In a native condition, Purkinje cells generate complex spikes in response to CF activation (Llinás and Walton, 1998). To see the effect of the Ca^{2+} channel mutations on the firing pattern of Purkinje cells, complex spikes were recorded in a current-clamp mode. Climbing fiber stimulation could evoke complex spikes in *tg* and tg^{rol}, and no obvious changes were observed (data not shown).

Ca^{2+} channel subtypes in CF-PC synapses

Previous studies showed that both P/Q- and N-type channels are present at CF terminals and play a critical role in neurotransmitter release and that the P/Q-type channel contributes more (70–90%) to the CF-PC synaptic transmission than the N-type channel (Regehr and Mintz, 1994; Doroshenko et al., 1997). Similar to earlier findings in rat cerebellum, application of 0.2 μM ω-Aga-IVA to the slices of wt partially blocked CF-EPSCs (Fig. 5*A*,*C*; Table 4). CF-EPSCs were reduced by ~50% of the baseline. On the other hand, application of 3 μM ω-CgTx reduced CF-EPSC by ~10% (Fig. 5*B*,*D*). Coapplication of 0.2 μM ω-Aga-IVA and 3 μM ω-CgTx eliminated the bulk of the synaptic current, leaving a small component (~10%) (Fig. 5*E*). Because the remaining component was not influenced by nifedipine (5 μM), it is likely to be an R-type channel-dependent component. These results demonstrate that among the P/Q-, N-, and presumed R-type Ca^{2+} channels, the P/Q-type Ca^{2+} channel plays a predominant role in the CF-PC synaptic transmission.

When the same set of experiments was performed on *tg* and tg^{rol} slices, clear alterations in toxin sensitivity were observed. In contrast to the large decrease in CF-EPSCs by ω-Aga-IVA in wt, there was only a small reduction in CF-EPSC amplitude in *tg* and tg^{rol} (Fig. 5*A*,*C*; Table 4). Application of ω-CgTx caused a large decrease in CF-EPSC amplitude in *tg* and tg^{rol} (Fig. 5*B*,*D*). Subsequent coapplication of 0.2 μM ω-Aga-IVA and 3 μM ω-CgTx further reduced CF-EPSCs, but the remaining component was much larger in *tg* than in wt (Fig. 5*E*). This component was not influenced by nifedipine (5 μM).

The relative contribution of Ca^{2+} channel subtypes was estimated using the power function, as for the PF-EPSCs (Table 4). The presumed R-type fraction is unexpectedly large, and the sum of the estimated fraction is far below unity. These unexpected estimates may be attributable to deviation from the power relation caused by saturation of Ca^{2+} binding sites. When the saturation effect is taken into account, the relationship between Ca^{2+} influx and EPSC can be described by the Hill's equation. The subtype fractions estimated using the Hill's equation were more consistent with earlier reports (Momiyama and Koga, 2001) (Table 4). In either model, the P/Q-type fraction was not so predominant as in the PF-PC synapses. The presumed R-type played a major role in wt, and its fraction, together with the N-type fraction, was increased in *tg*.

To test the validity of the estimation of Ca^{2+} channel fractions using the power relation or the Hill's equation, the effect on EPSC amplitude of lowering the external Ca^{2+} concentration was studied (Fig. 6). The PF-EPSC amplitude was very sensitive to lowering the external Ca^{2+} concentration. When the normalized PF-EPSC amplitude was fit by a power relation, the m value was 1.7, significantly lower than the commonly used value (3 ~ 4). The normalized CF-EPSC was well fit by the Hill's equation, with the power factor $m = 3.8$ and the relative half-saturation concentration $d = 0.29$, which is approximately half the value used in the toxin experiments ($d = 0.6$).

Table 3. Basic properties of CF-EPSCs in mutant mice

	Amplitude (pA)	Decay time constant (msec)	10–90% Rise time (msec)	Paired-pulse ratio (%)
Mice (P14–20)				
wt	787.7 ± 55.9 (40)	11.6 ± 0.5 (39)	0.41 ± 0.02 (14)	75.0 ± 2.3 (17)
tg	793.2 ± 61.4 (30)	11.1 ± 0.6 (14)	0.39 ± 0.04 (10)	82.1 ± 1.4* (10)
tg^{rol}	1149 ± 67.5* (31)	15.7 ± 1.0* (10)	0.39 ± 0.02 (10)	77.6 ± 2.2 (10)
Mice (P28–32)				
wt	841.1 ± 52.5 (10)	12.7 ± 0.6 (6)	0.34 ± 0.01 (6)	77.2 ± 1.8 (10)
tg	841.9 ± 91.7 (10)	12.3 ± 1.5 (9)	0.48 ± 0.04 (10)	87.2 ± 1.1* (10)

All data were expressed as mean ± SEM. Numbers of the recorded Purkinje cells are shown in parentheses. The decay time constant was obtained by fitting the EPSC decay with a single exponential. Paired-pulse ratio is second EPSC/first EPSC. Interpulse interval is 50 msec for CF-EPSCs. *$p < 0.05$.

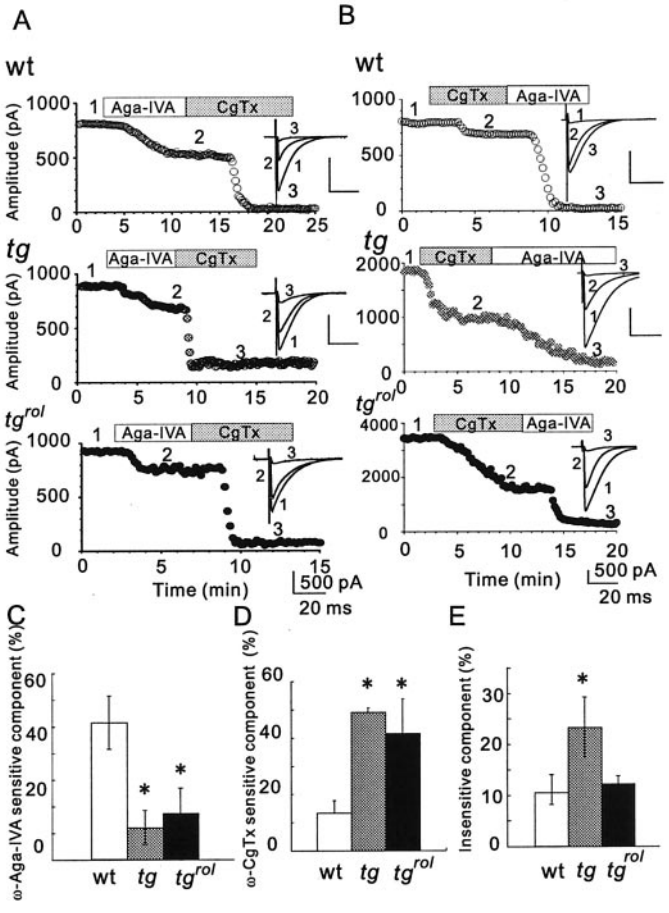

Figure 5. Toxin sensitivity of CF-EPSC. *A*, *B*, Time course of the peak CF-EPSC amplitude in response to application of 0.2 μM ω-Aga-IVA and 3 μM ω-CgTx (*A*) and to application of those blockers in the reverse order (*B*). *Insets* show current traces at the time indicated by the *numbers*. Each trace is an average of five recordings. *C*, *D*, The ω-Aga-IVA-sensitive (*C*) and the ω-CgTx-sensitive (*D*) components (mean ± SEM) of CF-EPSC of wt, *tg*, and tg^{rol} from three to six measurements. *E*, The remaining components after application of ω-Aga-IVA and ω-CgTx from six to eight measurements. *$p < 0.05$.

Synaptic glutamate concentration was not increased in tg^{rol}

The enhanced CF-EPSC amplitude in tg^{rol} may result from an increased release of glutamate because of a change in the presynaptic Ca^{2+} channels. To test this possibility, we estimated the glutamate concentration in the synaptic cleft by measuring the suppressing effect on CF-EPSC of various concentrations of a partial AMPA receptor antagonist, γ-DGG (Wadiche and Jahr, 2001). We found no significant difference in the inhibitory potency of γ-DGG on CF-EPSCs among wt, *tg*, and tg^{rol} at all the antagonist concentrations tested (0.5–5.0 mM) (Fig. 7). These results suggest normal glutamate release from CF terminals in tg^{rol} mutant mice despite the increased CF-EPSCs.

Miniature CF-EPSCs

The CF-EPSC decay time constant of tg^{rol} was larger than that of wt and *tg.* There are two possibilities to explain the prolonged EPSC decay. Although CF stimulation usually generates synchronous neurotransmitter release at each synapse in wt mice, neurotransmitter release may be asynchronous in tg^{rol}, resulting in a prolonged decay time constant. The other possibility is that functional properties of the postsynaptic AMPA receptors are altered to cause a larger decay time constant. Except during early development, Purkinje cells are innervated by both parallel and climbing fibers, which makes it difficult to measure CF miniature currents in isolation. We circumvented this problem by evoking CF-EPSCs in the presence of Sr^{2+} (Silver et al., 1998). Sr^{2+} can substitute for Ca^{2+} in triggering neurotransmitter release, but it causes desynchronized release (Abdul-Ghani et al., 1996). Miniature CF-EPSCs observed in a time window of 200–300 msec after stimulation were collected and analyzed (Fig. 8*A*). The decay time constant of tg^{rol} miniature CF-EPSCs was clearly larger than those of wt and *tg* (Fig. 8*B*). The result is consistent with the prolonged decay time of macroscopic CF-EPSCs and suggests a functional alteration of postsynaptic AMPA receptors in tg^{rol}.

Enhanced AMPA sensitivity in tg^{rol} Purkinje cells

Because the prolonged decay time constant of whole-cell and miniature CF-EPSCs in tg^{rol} suggests a postsynaptic origin, whole-cell currents were examined in acutely dissociated Purkinje cells from wt, *tg*, and tg^{rol} mice in response to a glutamate receptor agonist. Cyclothiazide (100 μM) was always included in the external solution to reduce desensitization (Partin et al., 1993). Application of AMPA (1–300 μM) to Purkinje cells at a holding potential of −50 mV evoked rapidly activating inward currents at all cells tested. Measurements were made at the peak of the responses. Concentration–response relationships for AMPA-evoked currents were not significantly different between wt [EC_{50} 53.1 ± 5.3 μM; Hill coefficient 1.1; maximum current density (I_{max}) 252.2 ± 26.5 pA/pF; $n = 12$] and *tg* (EC_{50} 48.7 ± 6.4 μM; Hill coefficient 1.0; I_{max} 217.2 ± 12.3 pA/pF; $n = 9$) (Fig. 7*C*). In contrast, the relationship of tg^{rol} was shifted in the direction of lower concentrations compared with those of wt and *tg* (EC_{50} 15.2 ± 2.0 μM; $n = 8$), but there were no significant differences in

Table 4. CF-EPSC synaptic current fractions after application of Ca^{2+} channel-blocking toxins

Toxins applied	ω-Aga-IVA (*a*) [*a*]	ω-CgTx (*b*) [*b*]	ω-Aga-IVA + ω-CgTx (*c*) [*c*]	(*a* + *b* + *c*) [*a* + *b* + *c*]
wt	0.46 ± 0.07	0.83 ± 0.03	0.11 ± 0.03	
	(0.23) [0.46]	(0.06) [0.18]	(0.47) [0.34]	(0.76) [0.98]
tg	0.88 ± 0.06	0.51 ± 0.02	0.23 ± 0.07	
	(0.04) [0.18]	(0.20) [0.43]	(0.62) [0.43]	(0.86) [1.04]
tg^{rol}	0.83 ± 0.1	0.69 ± 0.06	0.12 ± 0.02	
	(0.06) [0.23]	(0.12) [0.33]	(0.50) [0.35]	(0.68) [0.91]

Each value represents mean ± SEM of three or four cells. Numbers in parentheses (*a–c*) and brackets [*a–c*] are the estimated fractions of the Ca^{2+} channel subtypes, using the third power relation and the Hill's equation, respectively.

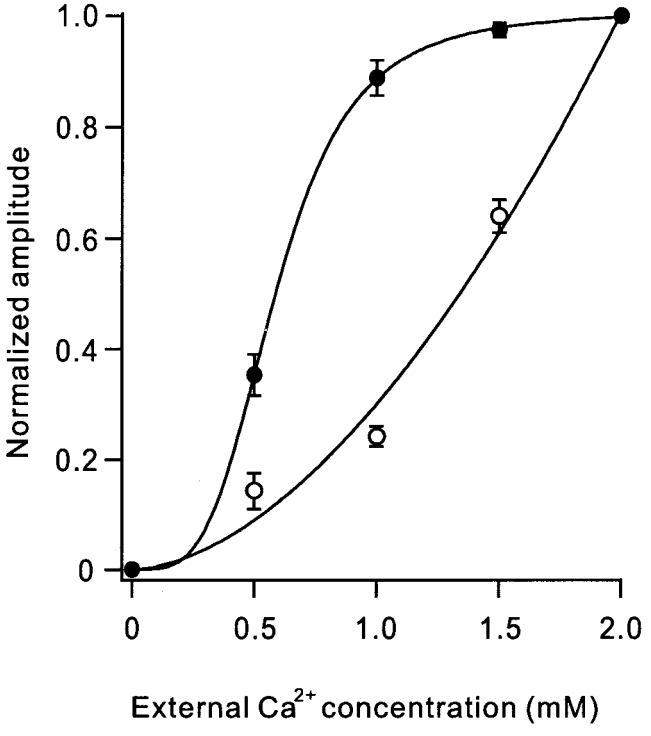

Figure 6. Effect of lowering the external Ca^{2+} concentration on EPSC amplitude. PF-EPSC amplitude (○) and CF-EPSC amplitude (●) were plotted as a function of the external Ca^{2+} concentration. The current amplitude was normalized to that at 2 mM external Ca^{2+}. Values are presented as mean ± SEM from five measurements each. PF-EPSC amplitude was fit by a power relation, $y = 0.30 * x^m$, where $m = 1.75$. CF-EPSC was fit by the Hill's equation, $y = 1.0068 * x^m/(x^m + d'^m)$, where $m = 3.78$ and $d' = 0.59$. The relative half-saturation concentration $d = 0.59$ mM/2 mM = 0.29.

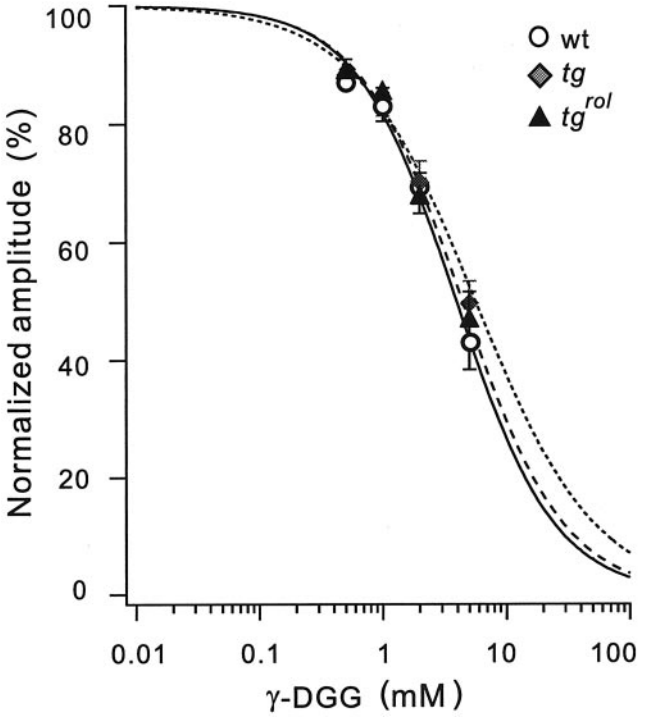

Figure 7. Effects of a partial AMPA receptor antagonist γ-DGG on CF-EPSCs. The graph shows concentration–inhibition curves for wt (*white circles*), *tg* (*gray diamonds*), and tg^{rol} (*black triangles*). The ordinate in the graph indicates percentage of the control CF-EPSC amplitude after application of γ-DGG. Values are presented as mean ± SEM from three to five measurements. The curves were fit by the Hill's equation. The half inhibitory concentrations were 3.94 ± 0.36 mM in wt, 4.98 ± 2.26 mM in *tg*, and 4.80 ± 0.43 mM in tg^{rol}.

Hill coefficient (1.17 ± 0.03) or I_{max} value (247.9 ± 51.7 pA/pF). These results suggest that the increase in the CF-PC response in tg^{rol} mice is caused at least partly by hypersensitivity of the AMPA receptors.

DISCUSSION

Cerebellar ataxia caused by P/Q-type Ca^{2+} channel mutations

Ataxia is the common symptom among the Ca^{2+} channel α_{1A} subunit mutant mice. Although loss of cerebellar neurons was reported in tg^{la}, there is no conclusive evidence to indicate neuronal death or degeneration in *tg* and tg^{rol}. Previous results suggested that the degree of deviation of the P/Q-type Ca^{2+} channel function in Purkinje cells was somewhat correlated with severity of ataxia in mutant strains (Wakamori et al., 1998; Mori et al., 2000). The P/Q-type Ca^{2+} channel current in Purkinje cells was reduced by ~60% in tg^{la}, whereas it was reduced by ~40% in *tg* and tg^{rol}. In tg^{rol}, however, the positive shift in voltage dependence of activation would further reduce the Ca^{2+} influx in native conditions in the brain.

Reduced PF-EPSCs and onset of ataxia

PF stimulation was consistently less effective in eliciting PF-EPSCs in ataxic *tg* and tg^{rol} than wt. Moreover, although P14–20 non-ataxic *tg* mice showed a mild reduction in PF-EPSC amplitude, clearly ataxic *tg* mice at P28–35 exhibited a more dramatic reduction, indicating a close relationship between impairment of the PF-PC synaptic transmission and cerebellar ataxia. The present results are consistent with the previous reports that ataxia

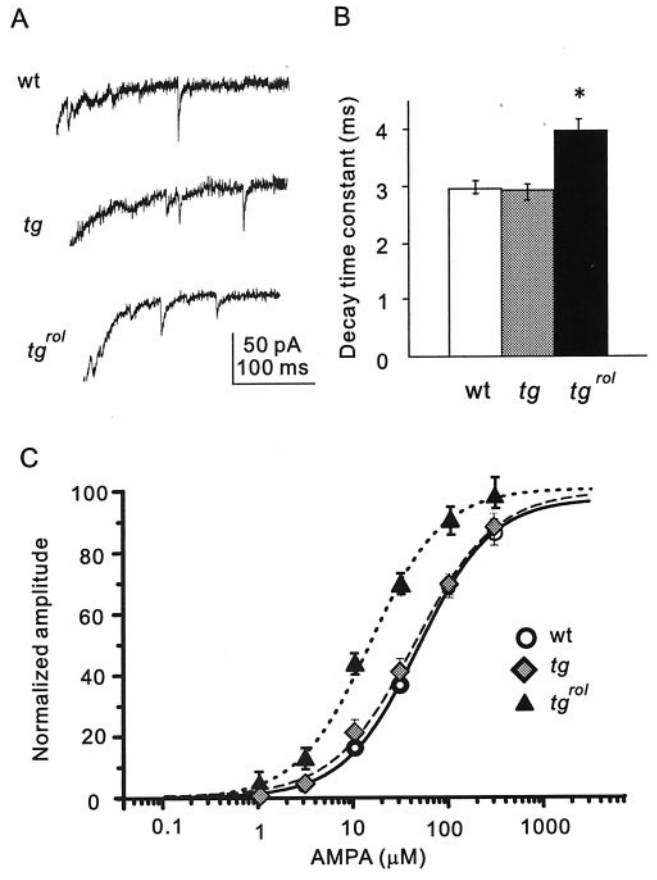

Figure 8. Altered postsynaptic glutamate sensitivity. *A*, Traces of miniature CF-EPSCs in response to CF stimulation, recorded from wt, *tg*, and tg^{rol} Purkinje cells in the presence of extracellular Sr^{2+}. Peak CF-EPSC was cropped to illustrate asynchronous quantal events in the tail. *B*, The decay time constants (mean ± SEM) of wt, *tg*, and tg^{rol}; 190–270 events were averaged. *C*, The AMPA concentration–response curves of wt (*white circles*), *tg* (*gray diamonds*), and tg^{rol} (*black triangles*). Data from each cell were normalized to the I_{max} value obtained from the Hill equation. Values are presented as mean ± SEM from 8–12 measurements.

is associated with dysfunction of the PF-PC system in *stargazer* mice (Letts et al., 1998; Hashimoto et al., 1999), *waggler* mice (Chen et al., 1999), and glutamate receptor (GluR)δ2 knock-out mice (Kurihara et al., 1997). These studies, however, have provided no clue about the temporal relationship between the PF-PC synaptic dysfunction and the onset of ataxia. Our results of the impaired PF response suggest that the dysfunction of the PF-PC synapse underlies cerebellar ataxia.

Purkinje cell firing of simple spikes normally ranges from 50 to 150 Hz depending on the strength of PF inputs (Ebner, 1998). The frequency of simple spikes is considered to encode centrally generated behaviors. In fact, voluntary eye or limb movements are associated with a marked change in simple spike frequency. Moreover, the PF-PC synapse can undergo long-term modifications in synaptic strength, and such plasticity has been suggested to underlie motor learning (Ito, 1986). The dysfunction of PF-PC synaptic transmission in *tg* and tg^{rol} thus not only blocks the transmission of centrally encoded behaviors but also impairs fine tuning of the neural circuits.

Properties of PF-PC synapse in mutant mice

Application of ω-Aga-IVA abolished 80–90% of PF-PC synaptic transmission in wt and mutants. Although this value was smaller than a previously reported value (~99%) (Mintz et al., 1995), the results suggest that the P/Q-type channels remains predominant in *tg* and tg^{rol}. On the other hand, the ω-CgTx-sensitive component was relatively increased in *tg*. When the fractional contribution of Ca^{2+} channel subtypes to PF-EPSC was estimated using the power relationship, the P/Q-type fraction was approximately half (Table 2). Interestingly, the presumed R-type was the second major component in wt. In mutants, the N-type contribution was increased, but it remained a minor component. The R-type was likely the predominant Ca^{2+} channel subtype in mutant PF terminals.

PPF at the PF-PC synapse was increased in tg^{rol}, likely as a consequence of severely reduced Ca^{2+} influx. It is also possible, however, that other secondary effects of the mutations were involved. The previous ultrastructural analyses showed that the number of PF nerve terminals having multiple contacts with dendritic spines of Purkinje cells was increased in *tg* and tg^{rol} (Rhyu et al., 1999a,b). Such structural reorganization may also contribute to partially compensating for the reduction of neurotransmitter release per synaptic contact of *tg* and tg^{rol} Purkinje cells.

Paradoxically enhanced CF-EPSCs in tg^{rol}

Because the P/Q-type is the major Ca^{2+} channel in CF nerve terminals, we expected that CF-EPSCs would be significantly reduced in mutants. In this study, however, the mean of amplitude and the decay time constant of CF-EPSCs were unchanged in *tg*, and surprisingly, the CF-EPSC amplitude was significantly increased and the current decay was slower in tg^{rol}.

To uncover the mechanism of altered CF-EPSC in tg^{rol}, we estimated the glutamate concentration in the synaptic cleft and measured the decay time constant of miniature CF-EPSCs as well as AMPA sensitivity of acutely dissociated Purkinje cells. There was no significant increase in glutamate concentration. The decay time constant of tg^{rol} miniature CF-EPSCs was larger than those of wt and *tg*. The AMPA receptors of tg^{rol} showed a higher sensitivity to AMPA in the presence of cyclothiazide. Those results suggest that the enhanced CF-EPSCs with a slower decay are caused at least partly by postsynaptic mechanisms, although other mechanisms such as the increased number of synaptic contacts may also be involved. The CF-PC responses are mediated by the AMPA receptors (Llano et al., 1991). Because CF-EPSCs were completely insensitive to APV in *tg* and tg^{rol}, the alteration of CF-EPSCs in tg^{rol} is not attributable to aberrant expression of NMDA receptor channels. The AMPA receptors have four kinds of subunits (GluR1–4), and each subunit has two alternative splicing forms, flip and flop. Our preliminary *in situ* hybridization study showed that GluR2 and GluR3 were the predominant subunits in wt Purkinje cells, but no significant changes in the expression pattern of GluR1–4 were observed in mutants. Because the AMPA receptors composed of the flip forms have a higher agonist sensitivity, a slower current decay (Mosbacher et al., 1994), and a slower desensitization in the presence of cyclothiazide (Partin et al., 1994), it is conceivable that the flip forms of GluR2 and GluR3 are predominantly expressed in tg^{rol} CF-PC synapses. The subunit composition of the postsynaptic AMPA receptors may be altered through the reduction in Ca^{2+} influx to dendrites of Purkinje cells. It is interesting to note that the composition of the AMPA receptors in the PF-PC and CF-PC synapses is regulated differently, because the kinetics of PF-EPSC remained unchanged in tg^{rol}.

Properties of CF-PC synapses in mutant mice

To examine the possibility that other Ca^{2+} channel subtypes are upregulated in mutant CF nerve terminals, we estimated the contribution of the P/Q- and N-types to CF-EPSC using the Hill's equation (Table 4). The fractional contributions of the P/Q-, N-, and presumed R-types are ~45, 20, and 35%, respectively, in wt. In *tg* and *tg^{rol}*, the P/Q-type fraction decreased to ~20%, and the N-type component increased to >30%. Because direct measurement of the presynaptic Ca^{2+} concentration was not made, it is difficult to estimate absolute changes of the N- and presumed R-type components, but the elevated ratio of the N-type to the R-type strongly suggests that the N-type channel current is actually increased, especially in *tg*, and this increase certainly contributes to maintaining the CF-PC synaptic transmission. A similar change has been reported in hippocampal synapses of *tg* mice (Qian and Noebels, 2000). Interestingly, PPD was reduced in *tg* without affecting the CF-EPSC amplitude. This finding may suggest that Ca^{2+} exerts a different depressing effect, depending on the Ca^{2+} channel subtypes through which Ca^{2+} has entered into the cell.

Ca^{2+} channels switch developmentally from the N-type to the P/Q-type at various synapses (Iwasaki and Takahashi, 1998; Rosato Siri and Uchitel, 1999; Iwasaki et al., 2000). Although no data are available for the CF-PC synapses, the increased N-type component in *tg* and *tg^{rol}* may be regarded as delayed maturation, provided the CF-PC synapses physiologically undergo developmental switching. The notion of the deranged developmental switching is supported by the morphological observations that ectopic spines arise from proximal dendrites of *tg^{rol}* Purkinje cells (Rhyu et al., 1999b). Similar morphological structures were reported in early developmental stages (Altman and Bayer, 1997). Climbing fibers form synapses on the protuberances of Purkinje cell soma and stem dendrites. Furthermore, hyperspiny transformation of the proximal dendrites is observed in the cerebellum where neuronal activity is blocked (Bravin et al., 1999). Because Ca^{2+} functions as an indicator of neuronal activity, impaired Ca^{2+} influx into *tg^{rol}* Purkinje cell dendrites may cause the deranged development and formation of ectopic dendritic spines.

PF-PC and CF-PC synapses

In this study, the parallel and climbing fiber systems showed a marked difference in the effects caused by the mutations. Although the PF-PC synapses showed severe impairments, the CF-PC responses remained intact or even enhanced. As shown by the effects of lowering the external Ca^{2+} concentration (Fig. 6) and by paired-pulse responses (Figs. 2, 4), the PF-PC synapses have a rather low release probability in the normal range of Ca^{2+} concentration. The presynaptic Ca^{2+} concentration is far below the saturating level, and the relationship between the Ca^{2+} concentration and the neurotransmitter release can be reasonably described by the power relation. Thus, a small reduction in Ca^{2+} influx causes a great reduction in transmitter release. These conditions render the PF-PC synapses more vulnerable to alterations of the presynaptic Ca^{2+} channels. In contrast, the CF-PC synapses have the large number of release sites, large quantal size, and high release probability, all of which would ensure that transmission at the CF synaptic connection is highly reliable at low frequencies. Strong PPD seen at these synapses, along with little increase in CF-EPSC amplitude with elevated external Ca^{2+}, indicate that release probability is near maximal (Dittman and Regehr, 1998; Silver et al., 1998). Thus the different responses to the mutations of the PF-PC and CF-PC synapses are partly explained by the difference in the strength of synaptic connections. To support this notion, the mutant mice have practically intact neuromuscular transmission (Plomp et al., 2000), which is dependent on the P/Q-type Ca^{2+} channel and has a high safety margin.

Altered P/Q-type channel function and neurological phenotypes

Because the P/Q-type is the predominant Ca^{2+} channel type in the CNS, it is rather surprising that the neurological dysfunctions are mostly confined to the cerebellum. Besides ataxia, however, some of the mutant mice show additional symptoms, including absence seizures (Burgess and Noebels, 1999; Zwingman et al., 2001). It is interesting how the diversity of neurological phenotypes is generated. The present work indicates that different neuronal populations have different levels of tolerance for the functional deviation of the P/Q-type channel. One important factor is the intrinsic safety margin of the affected synapses as mentioned above. The other important factor is the compensatory mechanism. When the P/Q-type channel is defective, other types of Ca^{2+} channels, such as N- and R-types, compensate for the mutational effects, but it appears that different neurons show different flexibility for the compensatory mechanism. To support this notion, the study of the N-type Ca^{2+} channel-deficient mice demonstrated that the baroreflex mediated by the sympathetic nerve was abolished, whereas these knock-out mice appeared normal otherwise (Ino et al., 2001). Furthermore, some neurons show strong preference for Ca^{2+} channel subtypes (Poncer et al., 1997). Mutations of the P/Q-type Ca^{2+} channel would thus disproportionately affect some subsets of neurons and thereby disrupt the balance of neuronal excitation and inhibition. Such disruption of a finely tuned balance between excitatory and inhibitory networks may result in episodic neurological symptoms, which include episodic ataxia and hemiplegic migraine associated with human Ca^{2+} channel α_{1A} subunit mutations (Ophoff et al., 1996).

REFERENCES

Abdul-Ghani MA, Valiante TA, Pennefather PS (1996) Sr^{2+} and quantal events at excitatory synapses between mouse hippocampal neurons in culture. J Physiol (Lond) 496:113–125.

Aiba A, Kano M, Chen C, Stanton ME, Fox GD, Herrup K, Zwingman TA, Tonegawa S (1994) Deficient cerebellar long-term depression and impaired motor learning in mGluR1 mutant mice. Cell 79:377–388.

Altman J, Bayer SA (1997) Development of the cerebellar system. Boca Raton, FL: CRC.

Artalejo CR, Adams ME, Fox AP (1994) Three types of Ca^{2+} channel trigger secretion with different efficacies in chromaffin cells. Nature 367:72–76.

Bourinet E, Soong TW, Sutton K, Slaymaker S, Mathews E, Monteil A, Zamponi GW, Nargeot J, Snutch TP (1999) Splicing of α_{1A} subunit gene generates phenotypic variants of P- and Q-type calcium channels. Nat Neurosci 2:407–415.

Bravin M, Morando L, Vercelli A, Rossi F, Strata P (1999) Control of spine formation by electrical activity in the adult rat cerebellum. Proc Natl Acad Sci USA 96:1704–1709.

Burgess DL, Noebels JL (1999) Single gene defects in mice: the role of voltage-dependent calcium channels in absence models. Epilepsy Res 36:111–122.

Catterall WA (2000) Structure and regulation of voltage-gated Ca^{2+} channels. Annu Rev Cell Dev Biol 16:521–555.

Chen L, Bao S, Qiao X, Thompson RF (1999) Impaired cerebellar synapse maturation in waggler, a mutant mouse with a disrupted neuronal calcium channel γ subunit. Proc Natl Acad Sci USA 96:12132–12137.

Dittman JS, Regehr WG (1998) Calcium dependence and recovery kinetics of presynaptic depression at the climbing fiber to Purkinje cell synapse. J Neurosci 18:6147–6162.

Dodge Jr FA, Rahamimoff R (1967) Co-operative action of calcium ions in transmitter release at the neuromuscular junction. J Physiol (Lond) 193:419–432.

Doroshenko PA, Woppmann A, Miljanich G, Augustine GJ (1997) Pharmacologically distinct presynaptic calcium channels in cerebellar excitatory and inhibitory synapses. Neuropharmacology 36:865–872.
Ebner TJ (1998) A role for the cerebellum in the control of limb movement velocity. Curr Opin Neurobiol 8:762–769.
Edwards FA, Konnerth A, Sakmann B, Takahashi T (1989) A thin slice preparation for patch clamp recordings from neurones of the mammalian central nervous system. Pflügers Arch 414:600–612.
Fletcher CF, Lutz CM, O'Sullivan TN, Shaughnessy Jr JD, Hawkes R, Frankel WN, Copeland NG, Jenkins NA (1996) Absence epilepsy in tottering mutant mice is associated with calcium channel defects. Cell 87:607–617.
Ghosh A, Greenberg ME (1995) Calcium signaling in neurons: molecular mechanisms and cellular consequences. Science 268:239–247.
Green MC, Sidman RL (1962) Tottering: a neuromuscular mutation in the mouse. J Hered 53:233–237.
Hashimoto K, Fukaya M, Qiao X, Sakimura K, Watanabe M, Kano M (1999) Impairment of AMPA receptor function in cerebellar granule cells of ataxic mutant mouse stargazer. J Neurosci 19:6027–6036.
Herrup K, Wilczynski SL (1982) Cerebellar cell degeneration in the leaner mutant mouse. Neuroscience 7:2185–2196.
Hirning LD, Fox AP, McCleskey EW, Olivera BM, Thayer SA, Miller RJ, Tsien RW (1988) Dominant role of N-type Ca^{2+} channels in evoked release of norepinephrine from sympathetic neurons. Science 239:57–61.
Ino M, Yoshinaga T, Wakamori M, Miyamoto N, Takahashi E, Sonoda J, Kagaya T, Oki T, Nagasu T, Nishizawa Y, Tanaka I, Imoto K, Aizawa S, Koch S, Schwartz A, Niidome T, Sawada K, Mori Y (2001) Functional disorder of sympathetic nervous system in mice lacking α_{1B} subunit (Ca_v 2.2) of N-type calcium channel. Proc Natl Acad Sci USA 98:5323–5328.
Ito M (1986) Long-term depression as a memory process in the cerebellum. Neurosci Res 3:531–539.
Iwasaki S, Takahashi T (1998) Developmental changes in calcium channel types mediating synaptic transmission in rat auditory brainstem. J Physiol (Lond) 509:419–423.
Iwasaki S, Momiyama A, Uchitel OD, Takahashi T (2000) Developmental changes in calcium channel types mediating central synaptic transmission. J Neurosci 20:59–65.
Kano M, Hashimoto K, Chen C, Abeliovich A, Aiba A, Kurihara H, Watanabe M, Inoue Y, Tonegawa S (1995) Impaired synapse elimination during cerebellar development in PKC gamma mutant mice. Cell 83:1223–1231.
Konnerth A, Llano I, Armstrong CM (1990) Synaptic currents in cerebellar Purkinje cells. Proc Natl Acad Sci USA 87:2662–2665.
Kurihara H, Hashimoto K, Kano M, Takayama C, Sakimura K, Mishina M, Inoue Y, Watanabe M (1997) Impaired parallel fiber → Purkinje cell synapse stabilization during cerebellar development of mutant mice lacking the glutamate receptor δ2 subunit. J Neurosci 17:9613–9623.
Letts VA, Felix R, Biddlecome GH, Arikkath J, Mahaffey CL, Valenzuela A, Bartlett 2nd FS, Mori Y, Campbell KP, Frankel WN (1998) The mouse stargazer gene encodes a neuronal Ca^{2+}-channel gamma subunit. Nat Genet 19:340–347.
Llano I, Marty A, Armstrong CM, Konnerth A (1991) Synaptic- and agonist-induced excitatory currents of Purkinje cells in rat cerebellar slices. J Physiol (Lond) 434:183–213.
Llinás R, Walton D (1998) Cerebellum. In: The synaptic organization of the brain, Ed 4 (Shepherd GM, ed), pp 255–287. New York: Oxford UP.
Llinás R, Sugimori M, Lin JW, Cherksey B (1989) Blocking and isolation of a calcium channel from neurons in mammals and cephalopods utilizing a toxin fraction (FTX) from funnel-web spider poison. Proc Natl Acad Sci USA 86:1689–1693.
Mintz IM, Venema VJ, Swiderek KM, Lee TD, Bean BP, Adams ME (1992) P-type calcium channels blocked by the spider toxin ω-Aga-IVA. Nature 355:827–829.
Mintz IM, Sabatini BL, Regehr WG (1995) Calcium control of transmitter release at a cerebellar synapse. Neuron 15:675–688.
Momiyama T, Koga E (2001) Dopamine D_2-like receptors selectively block N-type Ca^{2+} channels to reduce GABA release onto rat striatal cholinergic interneurones. J Physiol (Lond) 533:479–492.
Mori Y, Friedrich T, Kim MS, Mikami A, Nakai J, Ruth P, Bosse E, Hofmann F, Flockerzi V, Furuichi T, Mikoshiba K, Imoto K, Tanabe T, Numa S (1991) Primary structure and functional expression from complementary DNA of a brain calcium channel. Nature 350:398–402.
Mori Y, Wakamori M, Oda S, Fletcher CF, Sekiguchi N, Mori E, Copeland NG, Jenkins NA, Matsushita K, Matsuyama Z, Imoto K (2000) Reduced voltage sensitivity of activation of P/Q-type Ca^{2+} channels is associated with the ataxic mouse mutation rolling Nagoya (tg^{rol}). J Neurosci 20:5654–5662.
Mosbacher J, Schoepfer R, Monyer H, Burnashev N, Seeburg PH, Ruppersberg JP (1994) A molecular determinant for submillisecond desensitization in glutamate receptors. Science 266:1059–1062.
Oda S (1973) The observation of rolling mouse Nagoya (rol), a new neurological mutant, and its maintenance. Jikken Dobutsu 22:281–288.
Ophoff RA, Terwindt GM, Vergouwe MN, van Eijk R, Oefner PJ, Hoffman SM, Lamerdin JE, Mohrenweiser HW, Bulman DE, Ferrari M, Haan J, Lindhout D, van Ommen GJ, Hofker MH, Ferrari MD, Frants RR (1996) Familial hemiplegic migraine and episodic ataxia type-2 are caused by mutations in the Ca^{2+} channel gene CACNL1A4. Cell 87:543–552.
Partin KM, Patneau DK, Winters CA, Mayer ML, Buonanno A (1993) Selective modulation of desensitization at AMPA versus kainate receptors by cyclothiazide and concanavalin A. Neuron 11:1069–1082.
Partin KM, Patneau DK, Mayer ML (1994) Cyclothiazide differentially modulates desensitization of α-amino-3-hydroxy-5-methyl-4-isozazolepropionic acid receptor splice variants. Mol Pharmacol 46:129–138.
Plomp JJ, Vergouwe MN, Van den Maagdenberg AM, Ferrari MD, Frants RR, Molenaar PC (2000) Abnormal transmitter release at neuromuscular junctions of mice carrying the tottering $\alpha_{1A}Ca^{2+}$ channel mutation. Brain 123:463–471.
Poncer JC, McKinney RA, Gähwiler BH, Thompson SM (1997) Either N- or P-type calcium channels mediate GABA release at distinct hippocampal inhibitory synapses. Neuron 18:463–472.
Qian J, Noebels JL (2000) Presynaptic Ca^{2+} influx at a mouse central synapse with Ca^{2+} channel subunit mutations. J Neurosci 20:163–170.
Regan LJ, Sah DW, Bean BP (1991) Ca^{2+} channels in rat central and peripheral neurons: high-threshold current resistant to dihydropyridine blockers and ω-conotoxin. Neuron 6:269–280.
Regehr WG, Mintz IM (1994) Participation of multiple calcium channel types in transmission at single climbing fiber to Purkinje cell synapses. Neuron 12:605–613.
Rhyu IJ, Abbott LC, Walker DB, Sotelo C (1999a) An ultrastructural study of granule cell/Purkinje cell synapses in tottering (*tg*/*tg*), leaner (tg^{la}/tg^{la}) and compound heterozygous tottering/leaner (*tg*/tg^{la}) mice. Neuroscience 90:717–728.
Rhyu IJ, Oda S, Uhm CS, Kim H, Suh YS, Abbott LC (1999b) Morphologic investigation of rolling mouse Nagoya (tg^{rol}/tg^{rol}) cerebellar Purkinje cells: an ataxic mutant, revisited. Neurosci Lett 266:49–52.
Rosato Siri MD, Uchitel OD (1999) Calcium channels coupled to neurotransmitter release at neonatal rat neuromuscular junctions. J Physiol (Lond) 514:533–540.
Sather WA, Tanabe T, Zhang JF, Mori Y, Adams ME, Tsien RW (1993) Distinctive biophysical and pharmacological properties of class A (BI) calcium channel alpha 1 subunits. Neuron 11:291–303.
Sidman RL, Green MC, Appel SH (1965) Catalog of the neurological mutants of the mouse. Cambridge, MA: Harvard UP.
Silver RA, Momiyama A, Cull-Candy SG (1998) Locus of frequency-dependent depression identified with multiple-probability fluctuation analysis at rat climbing fibre-Purkinje cell synapses. J Physiol (Lond) 510:881–902.
Stea A, Tomlinson WJ, Soong TW, Bourinet E, Dubel SJ, Vincent SR, Snutch TP (1994) Localization and functional properties of a rat brain alpha 1A calcium channel reflect similarities to neuronal Q- and P-type channels. Proc Natl Acad Sci USA 91:10576–10580.
Takahashi T, Momiyama A (1993) Different types of calcium channels mediate central synaptic transmission. Nature 366:156–158.
Tsien RW, Tsien RY (1990) Calcium channels, stores, and oscillations. Annu Rev Cell Biol 6:715–760.
Turner TJ, Adams ME, Dunlap K (1992) Calcium channels coupled to glutamate release identified by ω-Aga- IVA. Science 258:310–313.
Wadiche JI, Jahr CE (2001) Multivesicular release at climbing fiber-Purkinje cell synapses. Neuron 32:301–313.
Wakamori M, Hidaka H, Akaike N (1993) Hyperpolarizing muscarinic responses of freshly dissociated rat hippocampal CA1 neurones. J Physiol (Lond) 463:585–604.
Wakamori M, Yamazaki K, Matsunodaira H, Teramoto T, Tanaka I, Niidome T, Sawada K, Nishizawa Y, Sekiguchi N, Mori E, Mori Y, Imoto K (1998) Single tottering mutations responsible for the neuropathic phenotype of the P-type calcium channel. J Biol Chem 273:34857–34867.
Zhang JF, Randall AD, Ellinor PT, Horne WA, Sather WA, Tanabe T, Schwarz TL, Tsien RW (1993) Distinctive pharmacology and kinetics of cloned neuronal Ca^{2+} channels and their possible counterparts in mammalian CNS neurons. Neuropharmacology 32:1075–1088.
Zucker RS (1989) Short-term synaptic plasticity. Annu Rev Neurosci 12:13–31.
Zwingman TA, Neumann PE, Noebels JL, Herrup K (2001) Rocker is a new variant of the voltage-dependent calcium channel gene Cacna1a. J Neurosci 21:1169–1178.